Measurement of the residual stress tensor in a compact tension weld specimen

Experimental Mechanics
DOI 10.1007/s11340-012-9672-7

Measurement of the Residual Stress Tensor in a Compact Tension Weld Specimen

Y. Traore · S. Paddea · P.J. Bouchard · M.A. Gharghouri

Received: 22 February 2012 / Accepted: 24 August 2012

Abstract Neutron diffraction measurements have been performed to determine the full residual stress tensor along the expected crack path in an austenitic stainless steel (Esshete 1250) compact tension weld specimen. A destructive slitting method was then implemented on the same specimen to measure the stress intensity factor profile associated with the residual stress field as a function of crack length. Finally deformations of the cut surfaces were measured to determine a contour map of the residual stresses in the specimen prior to the cut. The distributions of transverse residual stress measured by the three techniques are in close agreement. A peak tensile stress in excess of 600 MPa was found to be associated with an electron beam weld used to attach an extension piece to the test sample, which had been extracted from a pipe manual metal arc butt weld. The neutron diffraction measurements show that exceptionally high residual stress triaxiality is present at crack depths likely to be used for creep crack growth testing and where a peak stress intensity factor of 35 MPa$\sqrt{m}$ was measured (crack depth of 21 mm). The neutron diffraction measurements identified maximum values of shear stress in the order of 50 MPa and showed that the principal stress directions were aligned to within ~20° of the specimen orthogonal axes. Furthermore it was confirmed that measurement of strains by neutron diffraction in just the three specimen orthogonal directions would have been sufficient to provide a reasonably accurate characterisation of the stress state in welded CT specimens.

Y. Traore (✉) · S. Paddea · P.J. Bouchard
The Open University,
Walton Hall,
Milton Keynes MK7 6AA, UK
e-mail: y.traore@open.ac.uk

M.A. Gharghouri
NRC Canadian Neutron Beam Centre,
Chalk River, Ontario K0J 1 J0, Canada

Keywords Full stress tensor · Neutron diffraction · Slitting · Contour method · Finite element method

Introduction

Austenitic stainless steels are widely used in the construction of pressure vessels and pipework for electrical power plants and for the chemical industry where operating temperatures up to 600 °C may prevail. For example, Esshete 1250 is a creep resistant high manganese (6.5 %) austenitic stainless steel that has been used in the boilers of advanced gas cooled reactor nuclear power stations in the UK.

Fusion welding is employed to fabricate stainless steel pipework systems and components, but this is an aggressive thermal process that introduces undesirable residual stresses into joints and structures [1–4]. Post-weld heat treatment of stainless steel welds to relieve residual stresses is generally not required by engineering construction codes because they introduce detrimental metallurgical effects (sigma phase precipitation). A solution heat treatment (at 1050 °C) is sometimes applied to shop-welded stainless steel components which eliminates all residual stresses, but this high temperature treatment is rarely feasible for welds made on-site. Stainless steel weldments thus frequently enter service duty in the as-welded state with large residual stresses present.

Stainless steel weldments that are exposed to high temperatures (>450 °C) are vulnerable to creep deformation and creep damage mechanisms. For example, thick-section weldments with poor heat affected zone (HAZ) creep properties (low creep ductility) and highly triaxial residual stresses have developed large creep cracks in-service [5]. Weldments are especially prone to in-service degradation because of inhomogeneous microstructures resulting in gradients in material properties, stress

Published online: 06 September 2012

concentrations (e.g., at the weld root and cap), welding defects and residual stresses. In general, failure of engineering structures is avoided by designing structures to established construction codes with ample safety margins, by using carefully selected materials, by controlling workmanship and by applying inspection processes. However, for high integrity applications where safety consequences are paramount, it may be necessary to apply fracture mechanics-based methods for assessing the life of structures [6, 7]. For high temperature assessments of this kind it is essential to have detailed knowledge of the creep crack growth properties in the region of concern.

Creep crack growth testing for homogeneous materials is often conducted according to the ASTM E1457-00 standard test procedure [8] using compact tension (CT) specimens. However, there is no standard test procedure for dealing with materials exhibiting microstructural inhomogeneity, such as at weldments. Creep crack growth tests of HAZ material adjacent to Esshete 1250 welds have been conducted recently by EDF Energy [9]. The test programme used composite CT specimens of standard dimensions made by electron beam welding parent metal extension pieces to samples extracted from a mock-up pipe weldment. Unexpectedly high creep crack growth rates and crack opening displacements were observed in these tests. The objective of the present work is to characterise the magnitude and nature of residual stresses in these composite test specimens.

Residual stresses remaining in CT samples extracted from large weldments have been studied in various materials [10–14]. In particular, Davies et al [10] measured residual stresses up to three times the yield strength of the parent material by neutron diffraction in a CT specimen containing a manual metal arc weld.

The present work characterises the residual stresses present in an Esshete 1250 CT weld specimen with an electron beam welded extension piece by applying three independent methods. Uniquely, the full residual stress tensor along the path of the crack in the HAZ of a manual metal arc weld is determined to assess the degree of triaxiality, the significance of shear stresses and the deviation of the principal stress directions from the component orthogonal axes. The stress intensity factor profile due to the residual stress field as a function of crack length is measured directly on the same specimen using the destructive slitting method. The deformations of the cut surfaces from the slitting measurement are then used to generate a contour map of the residual stresses present normal to the cut. Residual stress results from the neutron diffraction, slitting and contour methods are then compared and the implications of the results discussed.

Test Specimen

The T-shaped test coupon shown in Fig. 1 was made by electron beam (EB) welding a parent metal extension piece to a cross-weld sample extracted from a purpose-made pipe butt weld. The extension piece was added to the outer surface of the pipe sample so that a compact tension (CT) specimen of standard dimensions could be extracted for creep crack growth testing of HAZ material, as shown in Fig. 1. The T-shaped test coupon was 52.6 mm deep, 69.3 mm wide and 21.3 mm thick. The pipe was made from Esshete 1250, a high manganese (6.5 %) austenitic stainless steel that had previously experienced prolonged exposure to high temperature service conditions. The multi-pass pipe butt weld was made using a manual metal arc (MMA) process with 3.2, 4 and 5 mm diameter ESAB OK 69.86 electrodes. The compositions of the service-exposed parent metal and weld consumables are listed in Table 1. The extension piece, also made from Esshete 1250, came from a separate source. Tensile properties for the materials were supplied by EDF Energy. The 0.2 % and 1 % room temperature flow stress values for the parent material were 241.1 MPa and 370 MPa, respectively. The corresponding values for the MMA weld metal were 534.5 MPa and 563.9 MPa. The elastic properties of the parent materials and weld metal were assumed to be isotropic having a Young's modulus of 204.5 GPa and a Poisson's ratio of 0.29 at room temperature [9]. The mean linear intercept grain size of the ex-service pipe parent material was measured to be 43.5 μm.

The outline for a CT specimen of standard dimensions [8] with a thickness B=19 mm is marked on the photograph of the supplied coupon in Fig. 1. A plain rectangular block 47.5 mm (1.25 W) wide, 45.3 mm (1.2 W) deep and 21 mm thick was extracted from the composite coupon by wire electro-discharge machining

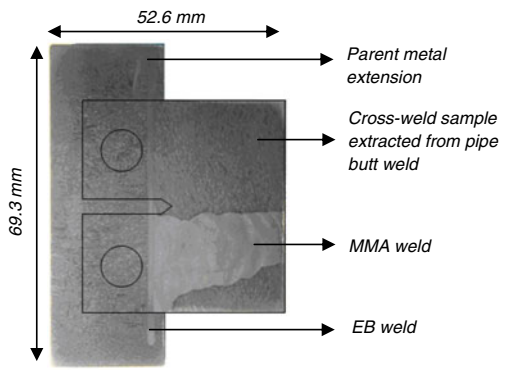

Fig. 1 Photograph of electron beam EB welded coupon (21.3 mm thick) prior to extracting a CT specimen blank (CT specimen outline marked showing proximity of the slot tip to the MMA weld)

Table 1 Chemical Compositions of the Esshete 1250 parent and weld metal in wt.%

	C	Si	Mn	P	S	Cr	Mo	Ni	Al	B	Co	Cu	Nb	Ti	V	W	N
Esshete 1250	0.09	0.49	6.5	0.019	0.007	15.1	1.03	10.1	<0.005	0.004	0.03	0.1	0.78	0.008	0.28	0.01	0.053
ESAB OK 69.86	0.11	0.35	7.1	0.021	0.003	16.4	1.12	8.9	<0.005	0.002	0.044	0.050	1.07	0.013	0.28	0.03	0.047

(EDM), see Fig. 2. The extracted block is referred to hereafter as the "CT blank." When determining levels of strain and stress in materials using neutron diffraction, it is essential to determine the stress-free lattice parameter in reference materials representative of where the lattice strain is being measured. This was achieved by removing a 5 mm thick slice from the CT blank face (labelled A in Fig. 2) by wire EDM and then extracting small, notionally stress-free, cubes at (*y,z*) positions corresponding to the neutron measurement locations (see neutron diffraction section for details). This machining operation reduced the thickness of the CT blank from 21 mm to 16 mm which is smaller than the standard CT thickness of 19 mm for W=38 mm. This compromise was an unavoidable consequence of the imperative to secure reliable measurements of the stress-free lattice parameters. Following removal of the 5 mm slice, face A of the CT blank was polished and etched to reveal the MMA weld fusion boundary. A datum line was then scribed on this surface 2 mm from the deepest point of penetration of the MMA weld passes, for the purpose of indicating the *yz* measurement plane for all three residual stress measurement techniques.

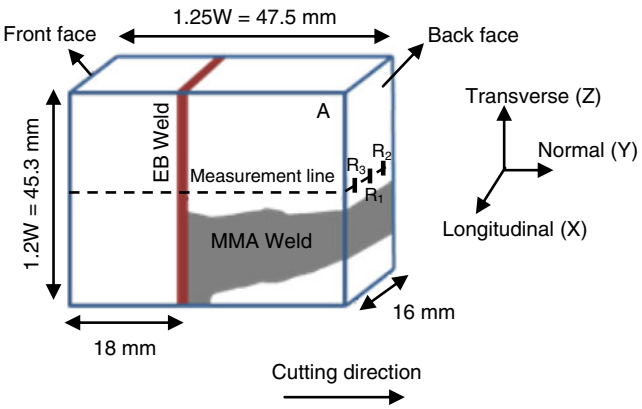

Fig. 2 Schematic drawing showing the final dimensions of the Esshete CT blank after machining to size for neutron diffraction, slitting and contour residual stress measurements. The measurement line/plane and locations of back-face strain gauges applied for the slitting are also indicated

Residual Stress Measurements

Residual stresses in the CT blank were measured by three techniques: neutron diffraction, slitting, and the contour method. Neutron diffraction [15] involves measuring the changes in lattice parameter due to the residual stresses. Slitting [16, 17] and the contour method [18] are destructive methods where residual strain is determined by measuring deformation after removal of material using strain gauges or other devices. The relieved stresses are then calculated by an inversion process using either numerical or analytical methods.

Neutron diffraction, a non-destructive measurement method, was first used to determine the full stress tensor along a line defined by the intersection of the mid-thickness *yz* plane and the mid-depth *yx* plane. It was decided to measure the full stress tensor because previous slitting measurements [11] on a similar CT specimen containing a MMA weld had revealed the presence of significant shear stresses in the plane of the crack near the fusion boundary; such stresses might make significant contributions to the stress intensity factor driving creep crack growth. In addition, for this case the authors judged it appropriate to challenge the universal assumption adopted in most engineering measurements that the principal directions align with the orthogonal directions determined by the weld geometry. Indeed, Winholtz and Krawitz [19], who determined the full stress tensor in a cylindrical weldment of HP-9-4-30 steel, reported that the principal stress directions were not aligned with the hoop, axial, and radial axes of the weld, but rather changed as a function of position within the weld.

Neutron Diffraction

Neutron diffraction relies on Bragg's Law (equation (1)), which relates the lattice plane spacing (d_{hkl}) for the family of crystallographic planes to the scattering angle ($2\theta_{hkl}$), that is the angle between the incident and diffracted neutron beams:

$$2d_{hkl}\sin\theta_{hkl} = n\lambda \tag{1}$$

where λ is the wavelength of the incident beam and n is an integer.

Neutron diffraction residual strain measurements in the CT blank were carried out on the L3 spectrometer of the Canadian Neutron Beam Centre, National Research Council, Canada. A monochromatic neutron beam was obtained using the {115} reflection of a germanium mosaic single crystal at a take-off angle of 89.28° (λ=1.529 Å). The neutrons' wavelength was determined using four diffraction peaks from a nickel powder standard sample. With this wavelength, the {311} reflection from the Esshete 1250 material occurred at a scattering angle $2\theta_{311}$=89.5° which, being close to 90°, provided optimal spatial resolution and avoided peak asymmetry arising as a result of axial divergence [20]. The {311} reflection was selected for the measurements as it has been shown to have low sensitivity to inter-granular strains in principal directions for metals with a face-centred cubic unit cell [21].

Stress-free lattice parameter (d_0) measurements

In measuring residual strain using the neutron diffraction method it is of paramount importance to obtain accurate measurements of the stress-free lattice parameter, d_0, because small changes in d_0 result in large changes in the corresponding stress. The approach taken here was to measure the lattice parameter in several stress-free reference cubes of dimensions (5×5×5) mm^3 EDM cut from the 5 mm thick slice removed from side A (see Fig. 2). This material was assumed to be representative of that at mid-thickness of the CT blank in the *yz* measurement plane. This size of cube was deliberately chosen to allow the proposed (2×2×2) mm^3 sampling volume to be increased if there turned out to be insufficient statistics/intensity during the experiment.

Since the d_0 measurements sampled a relatively small volume of material at the centre of the d_0 cubes, that is well away from the cut EDM surfaces, it is reasonable to assume that they were unaffected by any local residual stresses introduced by the wire EDM cutting process. Maximum residual stress levels that might remain in the d_0 reference cubes from the original residual stress field in the uncut component can be estimated from Fig. 3. This chart was determined from a two-dimensional finite element linear elastic stress analysis simulating application of a cosine distribution of stress to opposite edges of a rectilinear body and superposition of a negative cosine stress function throughout the body. It represents an extension of the theoretical solution for a cosine distribution applied to the edge of a semi-infinite body described by Nishioka et al [22] and Withers [2]. The chart gives the percentage of the maximum stress remaining in the cubes as a function of the ratio of one-half the cube's edge length to an assumed cosine residual

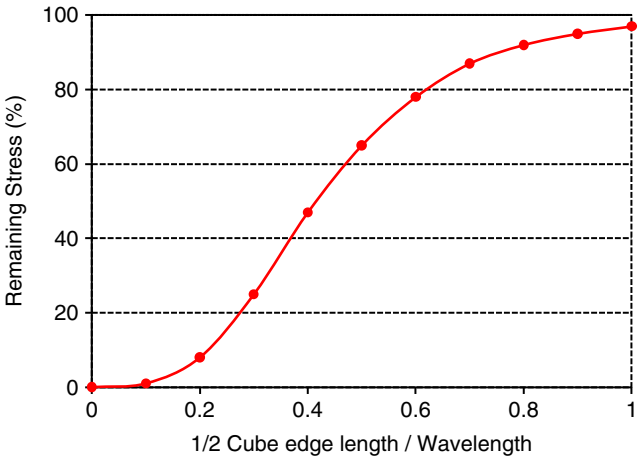

Fig. 3 Relationship for estimating the maximum remaining residual stress at the centre of a small cube (for neutron diffraction reference lattice parameter measurements), where wavelength relates to the length-scale of a cosine distribution residual stress in the original body

stress wavelength. Since the wavelengths of the longitudinal, normal and transverse residual stresses in the CT specimen are about 13, 20 and 25 mm respectively, the maximum stress likely to remain in the 5×5×5 mm^3 d_0 cubes close to the centre of the EB weld is estimated to be 22, 5 and 8 MPa respectively.

Each cube was rotated about an axis normal to the face of the cube on a simple device during the measurement, effectively averaging the lattice spacing over all specimen directions normal to the axis of rotation. This technique was adopted following the practice of Hosseinzadeh et al. [11] on a similar CT specimen where a wide scatter in measurements of the stress-free lattice parameter with orientation of the d_0 cube was observed which was attributed to imprecise positioning of the cubes relative to the neutron beam and the presence of large grains. Measurements were undertaken by rotating about all three cube axes and a single orientation independent value determined at each location. Although this pragmatic experimental procedure masks potential orientation dependence of d_0 owing to plastic anisotropy effects, which may well be present in the material close to the weld metal, this was judged to be a small effect as the {311} planes are least sensitive to plasticity induced microstresses. The gauge volume used for all measurements was (2×2×2) mm^3.

Lattice parameter (d) measurements

A total of 23 points were selected for measurement in the *yz* plane (defined by the scribed line on face A) at mid-thickness of the CT blank. The measurement points were spaced at 2 mm intervals with the first point located 1.41 mm from the CT blank front face (Fig. 2). The

spectrometer incident and scattered slits were carefully aligned with the centre of rotation of the sample table (the linear drives had a resolution of 0.005 mm). Neutron surface scans were then used to position the CT blank with respect to the fixed neutron gauge volume. The uncertainty in the measurement locations was in the order of 0.1 mm. In most neutron diffraction experiments, lattice strains are measured in 3 orthogonal directions irrespective of whether they are principal axes. Determination of the full strain tensor at a specific location requires measurement of the lattice strain in at least six independent directions. In this experiment, strains in eight different specimen directions were measured from which the full strain/stress tensors could be determined. The measurement directions are illustrated in Table 2. The sample was orientated in 3 different ways to measure the strain components listed. It is important to note that it was necessary to measure lattice strains along directions available using orientation 3, as the normal elastic strains along specimen directions available from orientations 1 and 2 depend on only a subset of the components of the full strain tensor. It would thus be impossible to solve for all of the strain components using only orientations 1 and 2, regardless of the number of normal strains measured. The eight measured normal strains yield an over-determined system that can be solved for the six independent components of the elastic strain tensor.

Data analysis

The measured {311} diffraction peaks were fitted to a Gaussian superposed on a constant background and the scattering angle, $2\theta_{311}$, was determined for each measurement point. The position-dependent lattice spacings, d_{311}, were then obtained from equation (1). Stress-free lattice parameters (d_0) were also determined in this way from measurements made on the stress-free cubes. For each measurement point, the corresponding strain was then calculated from the measured lattice parameters using equation (2).

$$\varepsilon = \frac{d - d_0}{d_0} \tag{2}$$

where ε, is the strain, d is the lattice parameter for the stressed material and d_0 is the stress free lattice parameter.

Assuming isotropic elasticity, the stresses in the CT blank for all directions can be calculated from the generalised Hooke's law:

$$\sigma_{ij} = \frac{E}{(1+\nu)}\left[\varepsilon_{ij} + \frac{\nu}{1-2\nu}\varepsilon_{kk}\delta_{ij}\right] \tag{3}$$

where σ_{ij} and ε_{ij} are the stress and strain on the face i and along the direction j of the sample, respectively, E is Young's modulus, ν is Poisson's ratio, ε_{kk} is the trace of the strain tensor and δ_{ij} is the Kronecker delta.

As mentioned earlier the full strain tensor can be determined when residual strains are measured in at least six different directions. By defining a Cartesian coordinate system related to the axes of the CT blank, one can define a rotated (primed) Cartesian coordinate system for each direction in which the normal strain is measured. In this case, the normal strain (ε'_{11}) along the x'_1 axis in the rotated coordinate system can be expressed in terms of the full strain tensor

Table 2 Specimen orientations and measurement directions

Orientation 1	Orientation 2	Orientation 3
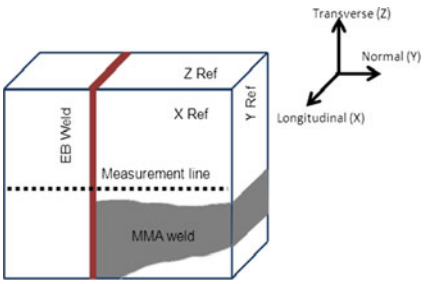	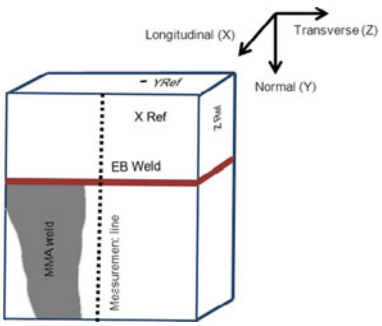	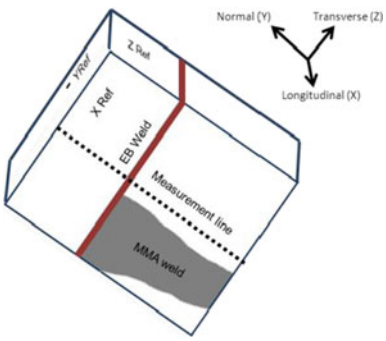
Perpendicular to Y_{Ref} (Normal) 25° rotation about Z 65° rotation about Z Perpendicular to X_{Ref} (Longitudinal)	Perpendicular to Z_{Ref} (Transverse) 25° rotation about Y	45° rotation about X (45° to Z and to Y) 25° rotation about the vertical axis

expressed in the original (unprimed) coordinate system (ε_{ij}) using the tensor transformation equation:

$$\varepsilon_{11}^{'} = a_{1i}a_{1j}\varepsilon_{ij} \tag{4}$$

In equation (4), $a_{1m} = \cos\left(X_1^{'}, X_m\right)$ is the direction cosine for the X'_1 axis of the rotated coordinate system with respect to the axis X_m of the unrotated specimen coordinate system. Equation (4) yields an expression for each measured normal lattice strain in terms of the components of the desired strain tensor. Since normal lattice strains were determined in eight different specimen directions, we obtain eight linear equations in six unknowns, to which we applied a least-squares procedure to determine the best possible values for the six unknown components of the strain tensor. Diffraction elastic constants for the {311} planes of 193 GPa and 0.3 were used in the analysis. These values were derived by factoring the macroscopic elastic properties of Esshete 1250 (204.5 GPa and 0.29) by the ratio of the {311} crystallographic to macroscopic elastic properties for Fe-Cr-Ni alloys containing 16–21%Cr, 2–3 % Mn and 10–14%Ni (derived using the model of Kroner [23] based on single crystal elastic constants C_{11}=208 GPa, C_{12}=133 GPa and C_{44}=121 GPa).

Slitting

Residual stress measurement by the slitting method (also known as the crack compliance method) is conducted by incrementally machining a narrow slot into a test component using a notionally stress-free cutting technique. The cut causes internal stresses to relax and the component to deform. The deformation response of the structure after each incremental cut is measured using strain gauges placed at optimal locations. The residual stresses acting along the cutting plane are then back-calculated from the measured deformation history using either a series expansion method or a fracture mechanics approach [16, 24, 25].

Sample preparation

The slitting method requires careful preparation before cutting by attaching strain gauges on both front and back faces of the test specimen. Measured strain data from the back face strain gauges alone are reported here because they give information about the stress distribution in the bulk of the specimen, whereas the front strain gauge results are only relevant for stresses within a couple of millimetres of the front face. Three strain gauges (R_1, R_2 and R_3) of type FLG-02-17 were carefully attached to the back face of the CT blank straddling the *yz* plane of measurement. Gauge R_1 was placed at mid-thickness of the specimen on the back face. Gauges R_2 and R_3 were centred 2.7 mm on either side of R_1 (Fig. 2). The gauge length of all the strain gauges was 1 mm. As the CT blank was submerged in water during the cutting process, a waterproofing protection system (clear silicone potting compound QSil 12) was applied to all the gauges.

Experimental procedure

Following attachment of the gauges, the CT blank was cut into two halves by an incremental wire EDM process. Just one side of the CT blank was clamped during cutting allowing the CT specimen to deform. The sample was submerged in de-ionised water for the wire EDM process. This minimises thermal strains and spark-induced cutting stresses, and facilitates removal of cut material by flushing. The slit was introduced incrementally using a 250 μm diameter wire. This relatively large diameter wire was selected in order to minimise the risk of wire breakage and also to reduce the concentration of stress at the cut tip; the latter is important because it can help to mitigate the risk of introducing plasticity during cutting. Two different cut increments were chosen: a 0.1 mm increment from 0 up to 8 mm and from 46 mm up to 47.4 mm and a 0.2 mm increment from 8 mm up to 46 mm. The corresponding strains for each cut length were recorded after stabilisation of gauge readings to within $1–2\times10^{-6}$ strain.

Stress back-calculation

Residual stresses can be determined from the measured back-face strains using different methods such as series expansion and the fracture mechanics approach [24]. Because the stress intensity factor (SIF) distribution in the CT blank was of particular interest for creep crack growth evaluation, the fracture mechanics approach was adopted for the data analysis. The advantage of this approach is that the SIF distribution as a function of the cut length can be directly and precisely determined without prior knowledge of the residual stresses [25] using see equation (5).

$$K_I = \frac{E'}{Z(a)}\frac{d\varepsilon}{da} \tag{5}$$

In this Equation, E' is the material's generalised Young's modulus (E'=E for plane stress and $E' = E/(1-\nu^2)$ for plane strain), ε is the measured strain at the cut depth *a,* and Z is the influence function. The influence function depends on the geometry of the component and the location of the strain measurement. As the present CT blank geometry did not match exactly with published solutions [26], the influence function was determined by finite element analysis.

The derived influence function was used to determine the SIF distribution, following which a weight function

approach (equation (6)) was applied to calculate the residual stress distribution [27]. Because of the CT blank dimensions, a plane strain condition was assumed to prevail.

$$K_I = \int_0^a h(x,a)\sigma_x dx \tag{6}$$

where $h(x, a)$ is the weight function, σ_x is the residual stress to be determined and a is the cut length.

Contour Method

The contour method is a destructive strain-relief technique for measuring residual stress [18] which relies on the principle of elastic superposition. The experimental procedure for the contour method involves first cutting the component of interest into two parts using a notionally stress-free cutting method. The deformation profiles of the newly cut surfaces are then measured and the data analysed to back-calculate the residual stress distribution normal to the surface that was present in the original uncut component.

Sample cutting

Wire EDM is currently the best machining technique for producing a parallel cut with flat surfaces suitable for applying the contour measurement method. Ideally, the sample should be clamped symmetrically on both sides of the cut during cutting in order to avoid introducing elastic and plastic cutting errors [18, 28]. However, in the present case only one side of the specimen was clamped in order to satisfy the boundary conditions required for the slitting measurement. In addition, the incremental cutting procedure required for the slitting measurement introduced some noise into the deformed surface profiles of the cut CT blank. Thus, the cutting conditions used for the slitting measurement were not ideal for producing a high quality contour residual stress measurement (see Discussion).

Cut surface profile measurements

Once the specimen was cut into two parts, the contours of the newly cut faces were measured using a Mitutoyo Crysta Plus 574 coordinate measuring machine (CMM) equipped with a 3 mm diameter Renishaw PH10M touch probe. The two cut parts being measured were placed side by side in the CMM workspace. The measurement spacing adopted in the thickness and length directions was 0.5 mm. Furthermore, the perimeters of both cut parts were measured as these profiles are used in the data analysis step.

Data analysis and stress back calculation

The processing of the raw deformation data involves several steps. First data from the two matching surfaces are averaged; this eliminates anti-symmetric errors (e.g., a curved cut) and the effect of shear stresses. Second, extreme outliers are removed from the dataset and the data are smoothed before mapping the deformation profile onto a finite element model of the cut component which is then used to calculate the residual stress. Different methods can be used to smooth the deformation data including 2-dimensional spline fitting, Fourier series or polynomial smoothing. In the present work two approaches were used: cubic spline fitting with different knot spacings and an implementation of a polynomial smoothing technique.

The spline fittng routine used in the present work was written in MatLab Software [29]. The routine uses the MatLab spline toolbox to join together piecewise polynomials at specified locations called “knots” which define the domain on which each polynomial is to be used. The spline toolbox also imposes both magnitude and slope continuity at the knots. The actual fitting of the spline is usually achieved by minimising the error between the data points and the fit. But the knot spacing chosen affects the resulting fitted splines. A low knot density (wide spacing) may lead to over smoothing of the measured data, while a high knot density may result in under smoothing. The maximum knot density is defined by the order of polynomial chosen (here cubic) and the measurement spacing. In practice some judgement is required, based on prior knowledge of the residual stress field, in order to select a spacing appropriate for the residual stress length-scales of interest.

The polynomial smoothing technique is an iterative technique in which a locally fitted bivariate polynomial is used to update the position of each measurement point [30]. The user selects the extent and the order of the fitted polynomial. The method requires the measured data to be meshed, but has the advantage that it may be easily applied to data on irregular physical domains.

A 3-dimensional finite element model based on the measured geometry (perimeter) of the CT blank was built using the ABAQUS code [31]. A total of 49370 linear hexahedral elements with reduced integration (C3D8R) were used with a (1×1) mm^2 regular mesh at the cut face. The material was assumed to be isotropic with a Young’s modulus of 204.5 GPa and Poisson’s ratio of 0.29 [9]. To avoid rigid body motion of the cut surface the model was restrained in two directions perpendicular to the cut surface. The smoothed measured deformation profile was applied as a boundary condition to the cut face and a linear elastic stress analysis was performed to calculate the residual stresses normal to the cut face. Providing the surface deformation

contour has been accurately idealised by the spline or polynomial smoothing process then the effective gauge area of the contour method can be related to the size of the linear elements used to represent it; which is (1×1) mm^2 for the present case.

Results

Neutron Diffraction

Stress-free lattice parameters (d_0) measured on small cubes extracted from the CT blank, as a function of angles (same angles depicted in Table 2) showed no systematic variation. As mentioned earlier, a rotating-sample technique was adopted to increase grain statistics. No significant variation in d_0 as a function of spin axis was found, see Fig. 4. However variations in d_0 between locations were found in the unaffected parent material, weld and locations within the HAZ of the MMA weld. Position-dependent average values of the spun d_0 were therefore used for stress calculations. The uncertainties in the measurements were of the order of 100 microstrain. Since direct strains were measured in 8 different specimen directions at each location, it was possible to apply a least-squares procedure to determine the best possible values for the 6 unknown components of the strain tensor. The optimised values were used for all the stress calculations.

Figure 5 shows the variation in longitudinal, normal, and transverse stresses along the mid-thickness measurement line in the plane *yz*. The uncertainty in the calculated stresses, based on the measurement of both d and d_0, was no greater than ±25 MPa. The longitudinal stress profile shows a maximum of ≈280 MPa at 19.4 mm from the front face of the CT blank. The peak stress in the transverse direction is tensile (≈ 640 MPa) and occurs at the same location. This peak is balanced by compressive stresses of up to ≈−190 MPa in the parent metal of the extension piece and in the HAZ of the MMA weld. The peak tensile stress in the normal direction is ≈230 MPa in the region of the electron beam weld. As expected, the normal stress is very small close to the front and back free surfaces (20 MPa and −25 MPa).

The full stress tensor, including orthogonal and shear components, was determined for each measurement point. Figure 6 illustrates the measured distributions of shear stresses across the specimen. It is evident that the shear stresses vary from about −50 to 50 MPa along the measurement line.

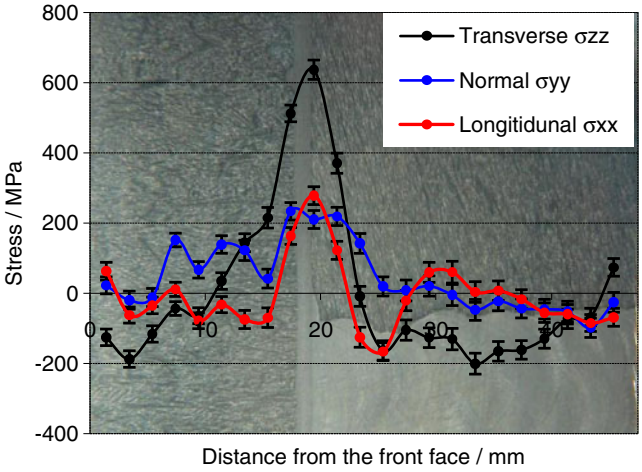

Fig. 5 Residual stress distributions in the longitudinal, normal and transverse directions along the mid-thickness line measured by neutron diffraction. A macrograph of the CT specimen has been superimposed on the graph to show clearly how the residual stresses correlate with the different zones in the specimen i.e. parent metal, EB weld and HAZ of the MMA weld

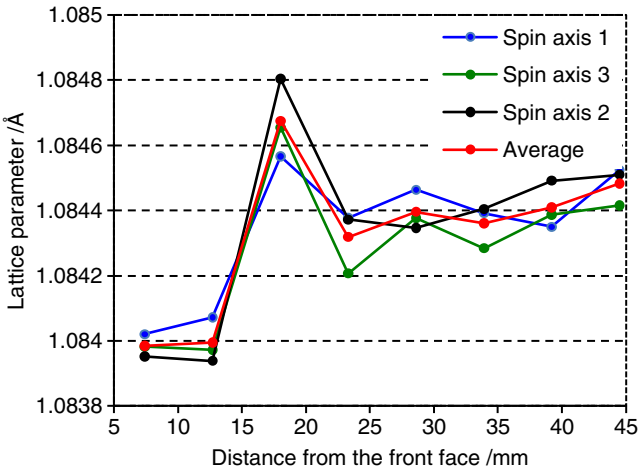

Fig. 4 Variation of stress-free lattice parameter with distance from the front face along the measurement line. The different spin axes represent rotations about the three cube-face axes. The uncertainties in these measurements were within ±100 microstrain

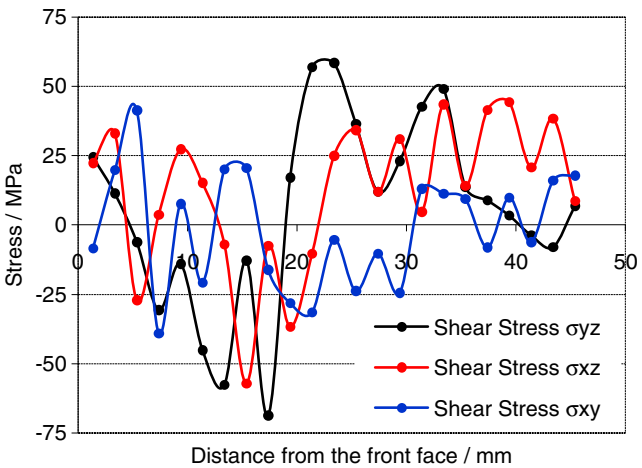

Fig. 6 Variation in shear stresses measured by neutron diffraction along the measurement line. The uncertainties in these measurements were of the order of ±15 MPa

Vector plots illustrating the deviations between the principal stress directions and the specimen orthogonal stress directions are provided in Fig. 7. The arrows along the measurement line represent the orientations of the 3 principal stresses (λ_1, λ_2 and λ_3) with respect to the orthogonal directions. Only directional information is represented in this figure (i.e. there is no implied information about stress magnitudes). Figure 7 shows that the principal directions were aligned with the specimen axes to within approximately 20 degrees. The principal stress values were within ±50 MPa of the corresponding orthogonal stress values shown in Fig. 5.

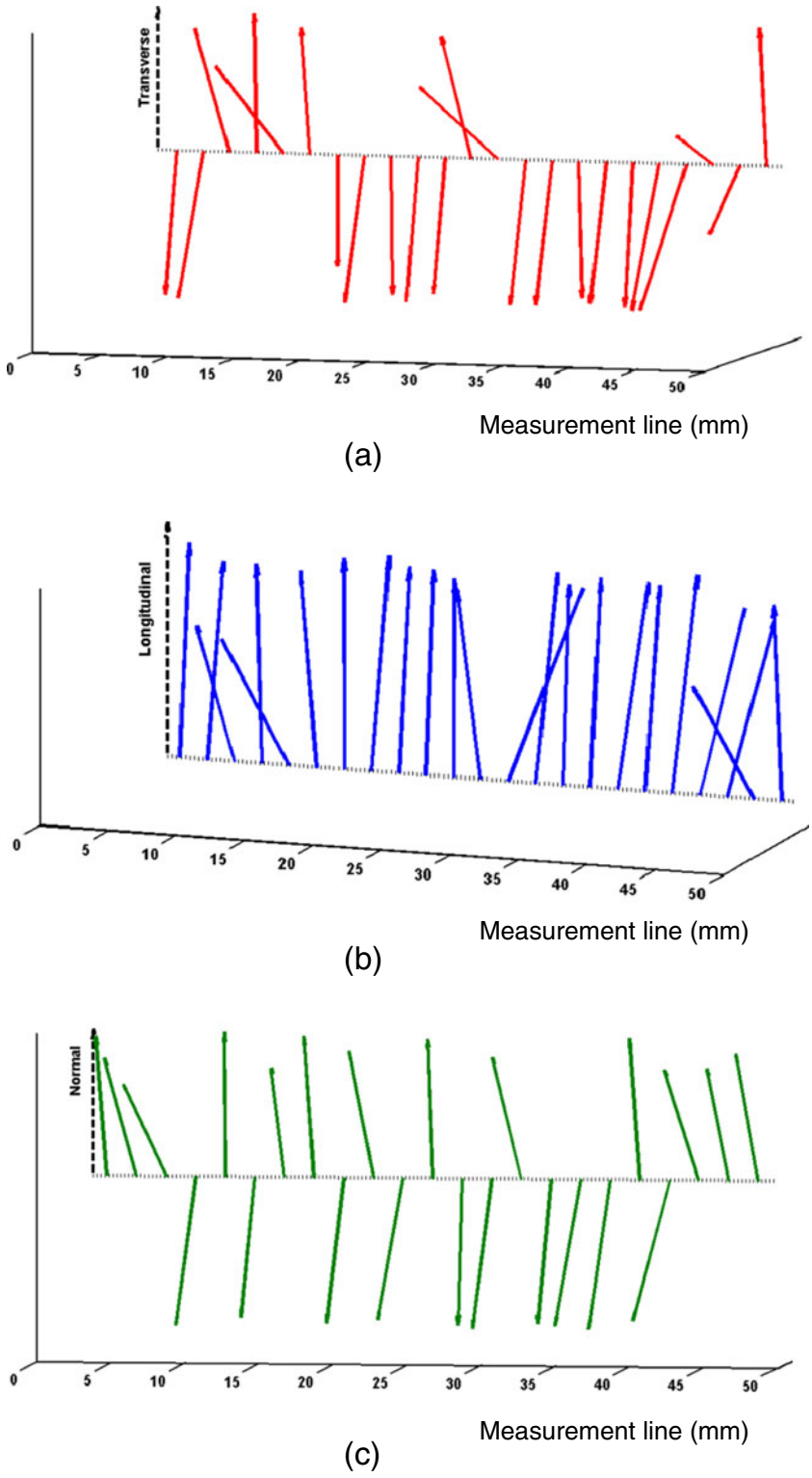

Fig. 7 Vector plots showing deviation of principal stress directions with specimen orthogonal stress directions; (**a**) transverse, (**b**) longitudinal and (**c**) normal

The distributions of hydrostatic and von Mises stress are shown in Fig. 8. Their peaks coincide at 19.4 mm from the front face of the CT blank with a magnitude of ≈370 MPa and ≈400 MPa, respectively. The high level of von Mises equivalent stress at this location, which is significantly greater than the parent metal yield stress, is likely to be associated with strain hardening introduced by the electron beam and MMA welds.

Slitting

The strain gauge data from the back-face of the CT blank were analysed using the fracture mechanics approach, as described earlier, to determine the distribution of mode I opening SIF as a function of the cut length. From Fig. 9 it is seen that the SIF rises to a peak value of 35 MPa√m for a slit depth of 21 mm from the CT blank front face. The distribution of transverse residual stress calculated from the measured SIF profile is shown in Fig. 10. The measured stress reaches a peak tensile magnitude of ≈590 MPa at a depth of 19 mm, which is in the region of the electron beam weld. Note that the slitting method gives values of the SIF and the transverse stress averaged across the thickness (*x*-direction) of the specimen.

Contour Method

Measured deformation data from the cut surfaces of the CT blank were processed using a conventional cubic spline approach with various knot spacings and the alternative second order polynomial smoothing approach described earlier. Figure 11 compares residual stress distributions determined using the two methods. Both maps show a similar tensile stress region around the electron beam weld balanced

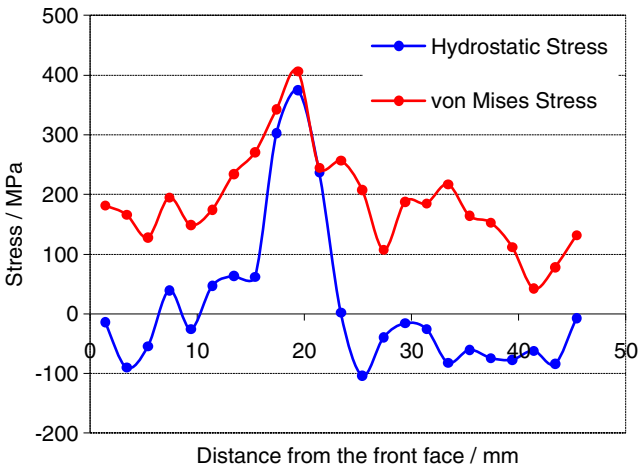

Fig. 8 Variation of hydrostatic and von Mises stresses measured by neutron diffraction along the measurement line. The uncertainties were of the order of ±15 MPa and ±35 MPa respectively

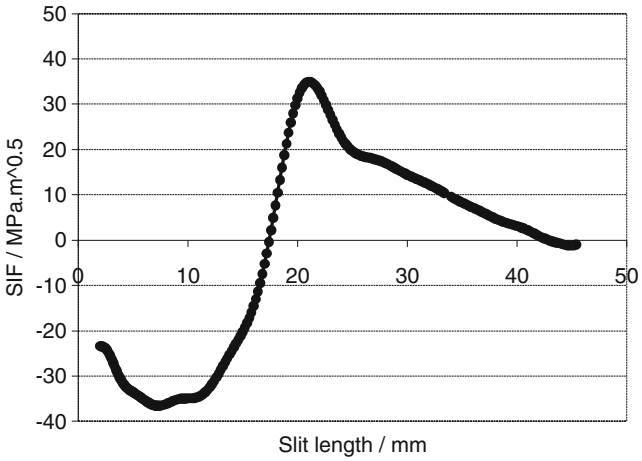

Fig. 9 Mode I stress intensity factor (SIF) as a function of cut length measured by the slitting method

by compressive stress fields in the parent material extension piece and in the HAZ of the MMA weld. Figure 12 shows more clearly how the stress profiles along the mid-thickness line correlate closely with each other. The polynomial smoothing approach is more robust in dealing with extrapolation of data to specimen edges, and therefore its results are used in the comparisons with slitting and neutron diffraction measurements which follow.

Discussion

A comparison of the distributions of transverse residual stress at mid-thickness of the measurement plane measured by neutron diffraction, slitting and contour methods is shown in Fig. 13. All three profiles follow the same trend with a peak tensile stress located around the electron beam weld region. The level of agreement of the three approaches

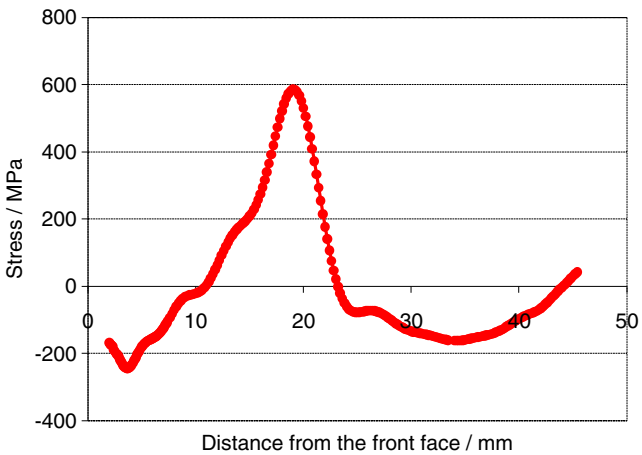

Fig. 10 Distribution of transverse (*z*-direction) membrane residual stress along the measurement plane derived from the slitting SIF profile

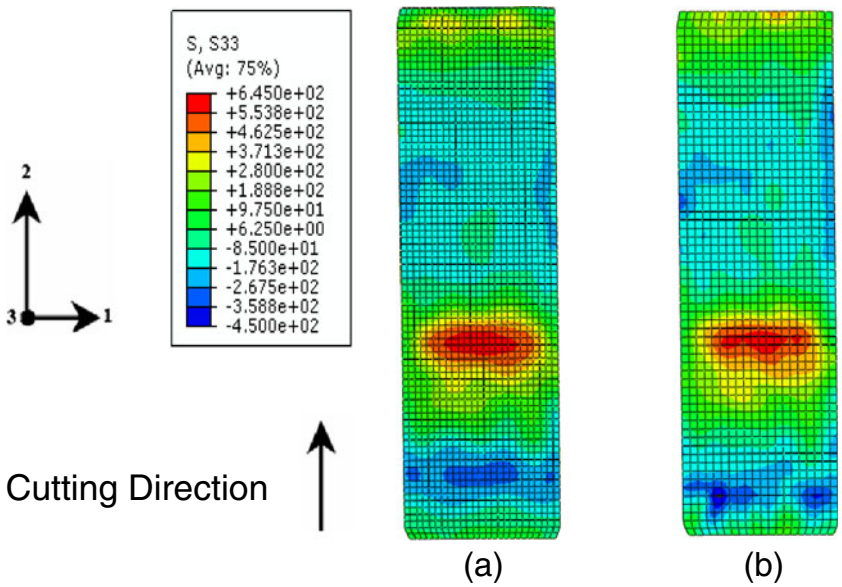

Fig. 11 Maps of measured transverse residual stress (normal to the cut faces) obtained from the contour method using different data analysis approaches: (**a**) cubic splines with a 3×3 mm^2 knot spacing, (**b**) second order polynomial smoothing

has been quantified. The contour method and the slitting peak tensile stress magnitudes are lower than the neutron diffraction peak tensile stress magnitude by 19 MPa (3 %) and 50 MPa (8 %), respectively. In the contour method result, a slight shift in the location of the tensile peak towards the CT front face is observed. The reduced peak tensile magnitude measured by slitting can be partially explained by the fact that the method measures averaged stresses across the thickness of the test specimen whereas the neutron diffraction measurements are averaged across a (2×2×2) mm^3 gauge volume. The difference in peak magnitudes between the slitting and contour stresses disappears when the latter are averaged across the thickness.

The potential significance of cutting plasticity on the accuracy of the slitting stresses was assessed using the recently published approach of Prime [12] which uses SIF data to estimate a percentage error in apparent measured stress knowing the material yield stress. The stress error is estimated to be about 15 % for a yield stress of 241 MPa (parent material 0.2 % proof stress) and 2 % for a yield stress of 430 MPa (work hardened yield stress in the region of the electron beam weld implied by the neutron diffraction measurements).

The outcome of the contour stress measurement is remarkably good considering the non-ideal restraint conditions (clamping on one side) and the incremental cutting procedure that had to be implemented for the slitting method measurement. Firm clamping on both sides of a contour measurement cut helps to control (reduce) the concentration of redistributed stress at the cut tip and thereby mitigate the

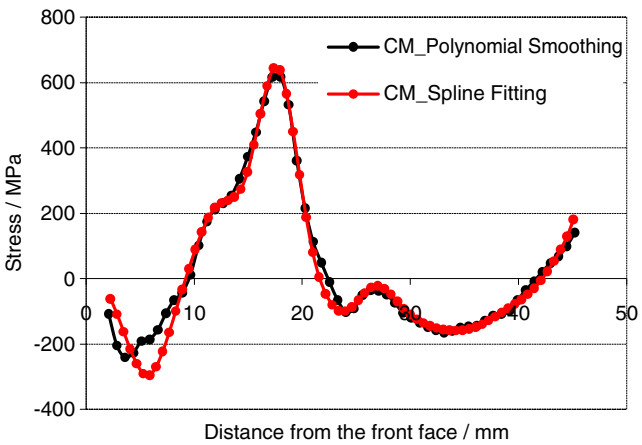

Fig. 12 Comparison of transverse residual stress profiles along the measurement line in the CT blank specimen measured by the contour method using different data analysis approaches

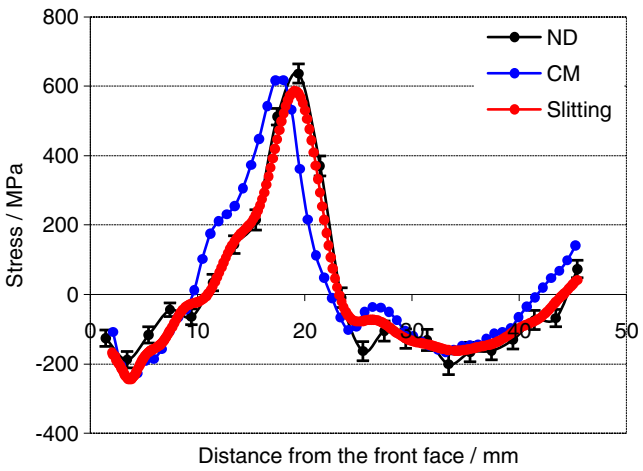

Fig. 13 Comparison of transverse residual stress profiles in the CT blank specimen measured by neutron diffraction, slitting and the contour method. The sampling volume for the neutron diffraction method is 2×2×2 mm^3, and effective gauge areas for the contour and slitting methods are 1×1 mm^2 and 16×0.2 mm^2 respectively

risk of plasticity occurring with the associated calculation errors [32]. The lack of restraint may explain why there is an apparent shift (about 2 mm) in the location of the peak stress in the contour measurement. Shifts in the peak stress location have been observed in previous contour measurements and attributed to plasticity during cutting [33]. On the other hand the differences might be associated with wire cutting artefacts which were observed at a cut depth of about 5 mm.

The hydrostatic and von Mises stress distributions calculated from the stress tensor results, shown in Fig. 8, can be used to calculate the residual stress triaxiality (ratio of hydrostatic to von Mises stresses) at any location along the measurement line. This parameter can have a significant effect on crack initiation and opening behaviour in ductile materials [34] and on fracture [35–37]. The measurements show that exceptionally high stress triaxiality is present (approaching unity) in the region between 17 and 22 mm from the CT blank front face. This corresponds almost exactly to the range of valid crack depths (15–21 mm) that would be tested in a creep crack growth test to ASTM E1457-00 [8]. The high triaxiality of the stress field in the region of the electron beam weld also explains why a large value of the transverse stress (640 MPa) was measured, exceeding the work hardened yield stress of 400 MPa implied by the measured von Mises stress.

The neutron diffraction full stress tensor results demonstrate that the maximum value of any shear stress in the specimen orthogonal coordinate system is in the order of 50 MPa and that the magnitude of the maximum principal stress is within ±50 MPa of the measured maximum specimen orthogonal stress. In addition, the vector plot (Fig. 7) illustrates how the principal stress directions lie within approximately 20^{o} of the specimen orthogonal directions. This evidence implies that measurement of strains in the three orthogonal specimen directions provides a reasonably accurate characterisation of the stress state in welded CT specimens.

It is the SIF that is of most significance for crack growth and fracture mechanics tests in CT specimens containing non-stress relieved welds. The slitting method result is particularly valuable because it provides a direct measure of the average SIF for a given uniform slit length. Here it is worth noting that machining the final CT geometry from a CT blank (i.e., the notch and starter slit) will introduce identical stress re-distribution and stress concentration at the crack tip to that observed in the slitting procedure. Thus the maximum measured SIF of 35 MPa$\sqrt{m}$ which occurs at a slit depth of 21 mm corresponds to the expected SIF for a crack depth to specimen width ratio, a_0/W, of 0.55 which is within the recommended range of crack sizes (a_0/W=0.4–0.55) specified in the creep crack growth test standard ASTM E1457-00 [8]. Therefore the SIF profile shown in Fig. 9 will have a large influence on crack growth behaviour in electron beam welded CT specimens, for example by creep, fatigue or stress corrosion.

The SIF distribution based on the stress profile determined from neutron diffraction measurements will be marginally greater than the slitting result (compare the stress profiles shown in Fig. 13). However, it would also be slightly less smooth owing to local periodic variations in stress along the HAZ of the MMA weld that appear to correlate with the fusion boundary profile of individual weld beads (see Fig. 5). A similar periodic variation adjacent to the MMA fusion line is evident in the shear stress components (σ_{yz} for example, shown in Fig. 6). However, the shear stresses vary by similar amounts from point to point in the parent material on the left side of the EB weld and therefore the apparent correlation may be a consequence of measurement scatter. The potential contribution to the total effective SIF from shear stresses could be estimated by determining the mode II and mode III SIFs associated with the shear stress profiles shown in Fig. 6. However, by inspection it is evident that these stress distributions have a self-equilibrated character and that the SIF for a 21 mm deep crack will be low [38].

The residual stress measurements show that electron beam welding an extension piece to a welded coupon introduces high magnitude triaxial residual stresses into the test sample. This will inevitably have a large effect on measured fatigue, fracture or creep crack growth behaviour. Where such specimens are used then the residual stress levels must be quantified using one or more of the methods described in this paper and then accounted for when interpreting test results. In this respect the slitting measurement is particularly useful because it quantifies the stress intensity factor directly. Evidently it would be better not to weld on such extension pieces in the first place. However, this is sometimes unavoidable when test materials which have been extracted from engineering components are of insufficient size to meet the dimensional requirements of accepted test standards. An alternative test strategy for these cases would be to design smaller scale non-standard test specimens; but the test results from such specimens would have to be supported by a development programme of comparative tests and supporting analysis.

Conclusions

1. High tensile residual stresses (>600 MPa) have been measured by three independent techniques in an Esshete 1250 CT specimen blank containing an EB weld. The stress field is dominated by highly triaxial residual stresses associated with an electron beam weld used to attach a parent metal extension piece so that standard CT dimensions could be achieved.

2. The distributions of transverse residual stress along the crack propagation plane measured by neutron diffraction, slitting and contour methods were in close agreement with each other with the peak stress from the contour method correlating to within 2 % of that measured by neutron diffraction.
3. The full residual stress tensor along the crack propagation plane of the CT specimen has been determined by neutron diffraction. The measurements demonstrate that the maximum value of any shear stress component in the specimen orthogonal coordinate system is in the order of 50 MPa and that the magnitude of the maximum principal stress is within ±50 MPa of the measured maximum specimen orthogonal stress. In addition, it has been shown that the principal stress directions lie within approximately 20^{o} of the specimen orthogonal directions. These results imply that measurement of strains by neutron diffraction in just three orthogonal specimen directions has provided a reasonably accurate characterisation of the stress state in welded CT specimens.
4. The neutron diffraction measurements show that exceptionally high residual stress triaxiality (hydrostatic to von Mises stress ratio approaching unity) is present at postulated crack depths (15–21 mm) in the CT specimen, ensuring that the conditions specified in the ASTM E1457-00 creep crack growth standard are met.
5. The stress intensity factor determined directly from the measured microstrains in the slitting method revealed a peak value of 35 MPa$\sqrt{m}$ at a crack depth of 21 mm. This corresponds to a crack depth to specimen width ratio, a_0/W, of 0.55, which is within the recommended range of crack sizes specified in the creep crack growth test standard ASTM E1457-00. Thus the SIF profile associated with the residual stresses in the CT weld specimen will have a large influence on crack growth behaviour for example by creep, fatigue or stress corrosion.

Acknowledgments The award of neutron beam time by NRC is gratefully acknowledged. The measurement work was funded by EDF Energy. The authors would like to thank Pete Ledgard and Stan Hiller for their invaluable help with the slitting measurement. P J Bouchard was supported by a Royal Society Industry Fellowship. This paper is published with the permission of EDF Energy.

References

1. Turski M, Bouchard PJ, Steuwer A, Withers PJ (2008) Residual stress driven creep cracking in AISI Type 316 stainless steel. Acta Mater 56(14):3598–3612
2. Withers PJ (2007) Residual stress and its role in failure. Rep Progr Phys 70(12):2211
3. Bouchard PJ (2007) Validated residual stress profiles for fracture assessments of stainless steel pipe girth welds. Int J Pres Ves Pip 84 (4):195–222
4. Bouchard PJ (2001) Residual stresses in lifing and structural integrity assessment. In: Buschow KHJ (ed) Encyclopaedia of Materials Science and Technology Pergamon, Oxford
5. Coleman M, Miller D, Stevens R (1998) Reheat cracking and strategies to assure integrity of Type 316 weld components. Paper presented at the International Conference on Integrity of High Temperature Welds, Nottingham, UK
6. R5, Assessment Procedure for the High Temperature Response of Structures (2003) 3 edn. British Energy Generation Ltd, Gloucester, UK
7. R6 Revision 4, Assessment of the Integrity of Structures Containing Defects (2010) British Energy Generation Ltd, Gloucester, UK
8. ASTM (2001) E 1457-00: standard test method for measurement of creep crack growth rates in metals. Annual Book of ASTM Standards 3(1):936–950
9. EDF_Energy (2010) AGR Materials Data Handbook. R66 Rev. 008. Gloucester, UK
10. Davies CM, Hughes D, Wimpory RC (2010) Measurements of Residual Stresses in 316 Stainless Steel Weldments. Paper presented at the ASME PVP Conference, Bellevue, Washington, USA
11. Hosseinzadh Torknezhad F, Bouchard PJ, James JA (2010) Measurements of residual stress in a welded compact tension specimen using the neutron diffraction and slitting techniques. Mater Sci Forum 652:210–215
12. Kerr M, Dunn D, Hill MR, Olson MD, Alexandreanu B, Willis E (2011) Effect of Residual Stress on Crack Growth Specimens Fabricated from Weld Metal Paper presented at the ASME PVP Conference Baltimore, Maryland, USA
13. Lewis SJ, Hossain S, Smith DJ, Truman CE, Hofmann M (2011) Determination of remnant residual stresses in fracture toughness specimens extracted from large components. Strain 47:e333–e343
14. Pratihar S, Stelmukh V, Hutchings MT, Fitzpatrick ME, Stuhr U, Edwards L (2006) Measurement of the residual stress field in MIG-welded Al-2024 and Al-7150 aluminium alloy compact tension specimens. Mater Sci Eng A 437(1):46–53
15. Hutchings MT, Withers PJ, Holden MT, Lorentzen T (eds) (2005) Introduction to the Characterization of Residual Stress by Neutron Diffraction. Taylor & Francis Group
16. Prime MB (1999) Residual Stress measurement by successive extension of a slot: the crack compliance method. Appl Mech Rev 52(2):75–96
17. Prime MB (2003) Experimental procedure for crack compliance (slitting) measurements of residual stress. LA-UR-03-8629, Los Alamos National Laboratory Report 2003
18. Prime MB (2001) Cross-sectional mapping of residual stresses by measuring the surface contour after a cut. J Eng Mater Tech 123 (2):162–168
19. Winholtz RA, Krawitz AD (1995) The relaxation of residual stresses with postweld heat treatment in a high-performance weld measured with neutron diffraction. Metall Mater Trans A 26A:1287–1295
20. Francis JA, Stone HJ, Kundu S, Bhadeshia HKDH, Rogge RB, Withers PJ, Karlsson L (2009) The effects of filler metal transformation temperature on residual stresses in a high strength steel weld. J Press Vess Technol 131(4):041401–041408
21. Non-destructive testing—Standard test method for determining residual stresses by neutron diffraction DD CEN ISO/TS 21432:2005 (2005)
22. Nishioka K, Hanabusa T, Fujiwara H (1974) Theory of the X-ray residual stress analysis. Scripta Metall 8:1349–1350
23. Kröner E (2003) Elastic moduli of perfectly disordered composite materials. J Mech Phys Solid 15(5):319–329

24. Prime (1999) Measuring residual stress and the resulting stress intensity factor in compact tension specimens. Fatig Fract Eng Mater Struct 22(3):195–204
25. Schindler H, Cheng W, Finnie I (1997) Experimental determination of stress intensity factors due to residual stresses. Exp Mech 37(3):272–277
26. Schindler HJ, Bertschinger P (1997) Some Steps Towards Automation of the Crack Compliance Method to Measure Residual Stress Distributions. Paper presented at the 5th Int. Conference on Res. Stress, Linköping, Sweden
27. Fett T, Munz D (eds) (1997) Stress intensity factors and weight functions. Computational Mechanics Publications, Southampton UK and Boston USA
28. Prime MB, Kastengren AL (2010) The contour method cutting assumption: error minimization and correction. Paper presented at the SEM Annual conference & exposition on experimental and applied mechanics Indianapolis, Indiana, USA
29. MATLAB (2009) Version 7.8.0 (R2009a). The MathWorks Inc
30. Vieira M, Shimada K, Furuhata T (2004) Smoothing of noisy laser scanner generated meshes using polynomial fitting and neighborhood erosion. J Mech Des 126(3):495–503
31. ABAQUS (2010) ABAQUS/Standard Documentation Version 6.10.2. ABAQUS, Inc 2010
32. Shin S (2005) FEM analysis of plasticity-induced error on measurement of welding residual stress by the contour method. J Mech Sci Technol 19(10):1885–1890. doi:10.1007/bf02984267
33. Bouchard PJ, Turski M, Smith MC (2009) Residual stress concentrations in a stainless steel slot-weld measured by the contour method and neutron diffraction. Paper presented at the ASME PVP Conference, Prague, Czech Republic
34. Mirza MS, Barton DC, Church P (1996) The effect of stress triaxiality and strain-rate on the fracture characteristics of ductile metals. J Mater Sci 31(2):453–461
35. Lee KS, Goldthorpe MR, Birkett RP, Sherry AH (2009) Residual stress and constraint effects on cleavage fracture in the transition temperature regime. Fatig Fract Eng Mater Struct 32(9):752–768
36. Panontin TL, Hill MR (1996) The effect of residual stresses on brittle and ductile fracture initiation predicted by micromechanical models. Int J Fract 82(4):317–333
37. Xu WG, Burdekin FM (1998) Effects of residual stresses on constraint and fracture behaviour of wide plates. Proc Math Phys Eng Sci 454(1977):2505–2528
38. Bouchard PJ, Budden PJ, Withers PJ (2012) Fourier basis for the engineering assessment of cracks in residual stress fields. Eng Fract Mech 91:37–50